Electropolymerized Poly(3,4-ethylenedioxythiophene) Coatings on Porous Carbon Electrodes for Electrochemical Separation of Metals

RESEARCH ARTICLE

Editor's Choice

ADVANCED MATERIALS INTERFACES
Open Access
www.advmatinterfaces.de

Electropolymerized Poly(3,4-ethylenedioxythiophene) Coatings on Porous Carbon Electrodes for Electrochemical Separation of Metals

*Emre B. Boz, Marcell Fritz, and Antoni Forner-Cuenca**

Electrode-assisted techniques are well suited for the separation of ions from solutions with reduced energy and chemical consumption. This emerging platform can benefit greatly from the convection enhanced and zero-gap reactor designs unlocked by macroporous electrodes, but immobilizing ion-selective layers on such complex 3D architectures is challenging. Electropolymerization of conductive polymers is proposed as a coating methodology to fabricate highly conformal coatings with electrochemically switchable ion-exchange functionality. To demonstrate this, the synthetic parameters, resulting morphology, and ionic separation performance of poly(3,4-ethylenedioxythiophene) (PEDOT) on commercially available carbon paper electrodes are studied. Electropolymerization of PEDOT in organic solvents results in rougher morphologies with high sensitivity to electrochemical protocols employed. When polymerized in aqueous solutions of poly(4-styrenesulfonate) (PSS^-), the resulting PEDOT/PSS blend polymer forms smooth coatings with a controllable thickness down to 0.1 µm. With appropriate voltage bias, PEDOT/PSS coated electrodes can take up and release Ni^{2+} in the presence of excess Na^+. Increasing the coating thickness decreases the adsorption capacity due to mass transfer limitations, and the maximum adsorption capacity for Ni^{2+} is reached for the thinnest coatings at 228 mg g^{-1}. Through a systematic study of PEDOT/PSS coated carbon paper, electropolymerization is identified to be a promising avenue for porous electrode functionalization.

1. Introduction

Decarbonization of the energy grid is gaining importance as global temperatures are rising and concerns over the energy security are growing.[1] Reaching net-zero emissions will require decarbonization of entire sectors, which puts more emphasis on renewable energy generation.[1] To this end, emerging technologies such as batteries, photovoltaics, and wind turbines are being integrated into the grid at an accelerating rate. However, these technologies rely on metals that are rare or have unequal distribution throughout the world.[2,3] The demand on these metals, also known as critical metals, is expected to grow over the coming years, resulting in increased mining, refining, and purification efforts.[3] Mining of metals and minerals threatens the environment and human health as it leads to habitat loss and mismanaged mining effluents leading to contamination of waters.[4,5] Mining of metals such as cobalt, nickel, and lithium also contributes to socioeconomic issues in developing countries.[2] Thus, there is a need for sustainable purification and extraction of these elements from secondary sources such as mining and manufacturing effluents, recycling products, and brines.[6–9] However, these secondary sources contain low concentration of critical elements in their ionic form, which makes their separation challenging and energy intensive with conventional methods such as filtration or sedimentation.[10]

Electrode-assisted processes are well suited for ionic separations involving dilute streams as electric field and charge compensation can be used as a driving force to mobilize and capture ions within the solution.[11] More importantly, the ability to change the affinity of the surface toward a metal ion with simple handles such as electric potential minimizes the use of recovery agents and the subsequent secondary pollution.[12] Electrode-assisted separation processes rely on the electrosorption phenomena where ions are immobilized on the electrode to balance the surface charge. A well-known example where electrosorption is utilized is capacitive deionization (CDI), which relies on the double layer formation on high surface area electrode materials such as activated carbons and carbon

E. B. Boz, M. Fritz, A. Forner-Cuenca
Electrochemical Materials and Systems
Department of Chemical Engineering and Chemistry
Eindhoven University of Technology
P.O. Box 513, Eindhoven 5600 MB, The Netherlands
E-mail: a.forner.cuenca@tue.nl

E. B. Boz, A. Forner-Cuenca
Eindhoven Institute for Renewable Energy Systems
Eindhoven University of Technology
P.O. Box 513, Eindhoven 5600 MB, The Netherlands

The ORCID identification number(s) for the author(s) of this article can be found under https://doi.org/10.1002/admi.202202497.

DOI: 10.1002/admi.202202497

aerogels.[13] Recently, the research interest for electrosorption-based metal ion separation is shifting towards Faradaic materials as, in comparison with purely capacitive materials, they often offer higher selectivity while lowering the energy required for separation.[14] Unlike CDI, Faradaic electrosorption is not limited to the surface of the electrode and can be performed on materials that can expel or ingress ions upon application of potential, and this process is aptly named as electrochemically switchable ion exchange (ESIX). Instead of immobilizing the metal ions in the double-layer region, ESIX materials interact with the target ion at a crystalline or polymeric site, allowing the bulk of the material to contribute to the separation process.[14,15]

Among ESIX materials, crystalline intercalation compounds such as $LiMnO_2$, $LiCoO_2$ and $LiFePO_4$ have been used for electrode-assisted separation of Li^+ from low-concentration brines.[16–18] Intercalation compounds such as Prussian blue analogs feature highly selective ion adsorption sites within their lattice and have been used to desalinate brackish waters and to separate valuable metals from aqueous solutions.[19–22] Redox-active polymers are another group of ESIX materials and their redox activity result from organic (e.g., nitroxide radicals, thiophene) or organometallic (e.g., metallocenes, metal-pyridine complexes) functional groups.[23–26] Redox-active polymers with pendant groups of ferrocene and cobaltocene have been shown to be promising for ESIX-based ionic separations with good selectivity owing to their unique electronic structure.[27,28] However, these crystalline intercalation compounds and metallocene-based polymers suffer from low electronic conductivity and/or have low film forming ability.[29,30] Unlike CDI electrodes where bottom-up electrode manufacturing is possible, ESIX materials have to be supported on a conductive scaffold and possibly blended with a conductive filler (e.g., carbon black).[31,32] The use of dense and planar scaffolds would fundamentally limit performance in electrochemical flow cells due to low surface area and inaccessible ion-exchange sites. Thus, ESIX-based separation platforms would benefit greatly from the implementation of macroporous electrodes as they offer forced convection through the electrode and enable zero-gap constructions with low internal resistances.[33] Commercially available macroporous electrodes such as carbon fiber-based cloths, felts and papers are ubiquitous for fuel cells and redox flow batteries and can be applied to support the active material for flow-enabled ESIX.[34,35] However, immobilizing these materials into macroporous electrodes is challenging with conventional ink-based coating methods (i.e., dip coating, drop casting, infiltration) as they lack control over the coating distribution, loading, and uniformity on the porous substrate, potentially resulting in pore clogging and underutilization of the active material.[36] Thus, it is necessary to develop techniques that offer accurate control over the coating properties and are compatible with porous electrodes and large-scale manufacturing.

Here, we explore the use of electropolymerization of a conductive polymer as a method to deposit conformal coatings on 3D porous electrodes with a complex architecture. Conductive polymers are a sub-group of redox-active polymers that can be polymerized directly on conductive scaffolds via the electropolymerization method. Electropolymerization proceeds by potential-induced radical generation near the surface of the electrode and their subsequent polymerization, which decreases the solubility of the polymer and causes rapid condensation and precipitation onto the electrode.[37] Since the polymerization reaction takes place even in the pore space, every surface of a porous scaffold can be coated with a layer of active material. As their name implies, conductive polymers are electrically conductive owing to the conjugation along the polymer backbone that results in an extended pi-network.[38] Consequently, they do not require an additive (commonly carbon black) to perform ESIX and can be even used as a conductive matrix for other ESIX materials.[39–44]

In this work, we study the polymerization of poly(3,4-ethylenedioxythiophene) (PEDOT) on carbon paper substrates (**Scheme 1**). We elect to use PEDOT as it is one of the most stable conductive polymers with industrial relevance.[45] Owing to its low cost, transparency, and high processability, PEDOT and its formulations have found extensive use as an electrode material in organic and dye-sensitized solar cells.[46–48] More recently, PEDOT has been investigated as an electrode (coating) for other energy applications such as Li-ion and metal-ion batteries, redox flow batteries, and supercapacitors.[49–53] Interested readers can refer to the extensive reviews on the properties and applications of this polymer.[54,55] PEDOT is a p-type conductive polymer where the reduced form of the polymer is neutral and the oxidized form is positively charged. For p-type conductive polymers, anions can be expelled and ingressed into the structure during the redox reactions to compensate for the polymer charge. However this ion exchange is not specific to anions, so cations and solvent molecules can be carried into the structure as well.[56,57] It is possible to tune this behavior by utilizing large dopant ions, such as polyanions, imparting permanent cation exchange property to the coating. Poly(4-styrenesulfonate) (PSS^-) is a polyanion that is popularly blended with PEDOT via chemical or electrochemical means.[54] When PEDOT is oxidized, the positive charges on the backbone are associated with the sulfonate units of the PSS^-. However, when PEDOT is reduced, these sulfonate groups associate with other cations in the solution to preserve the charge neutrality within the film (Scheme 1d). PSS^- cannot leave the blend structure easily as it is sterically hindered and, consequently, permanent cation exchange is observed in PEDOT/PSS.[58] Through electrochemical redox reactions of PEDOT, the PEDOT/PSS system acts as a cation exchanging ESIX material in solutions.

The electrochemical, morphological, and ion-exchange properties of the PEDOT coatings can be tuned based on the counterion, solvent, or the electropolymerization mode.[59–62] We hypothesize that applications that require a large surface area (e.g., enzyme immobilization, capacitors) may benefit from a porous and rough coating, while applications with significantly large liquid flow rates (e.g., flow cells) would benefit from smoother surfaces, thereby reducing the pumping requirements. Thus, it is critical to connect the synthetic parameters of PEDOT coatings on porous scaffolds to the final coating structure and morphology. In the first part of this work, we study the influence of the counterion type, solvent, and electropolymerization mode on the morphology of PEDOT when it is coated on a porous scaffold such as carbon paper. Second, we focus on the galvanostatic polymerization of PEDOT/PSS as the relevant system and draw inferences on the effect of polymerization conditions on the coating thickness. Third, we investigate

ADVANCED MATERIALS INTERFACES
Open Access
www.advmatinterfaces.de

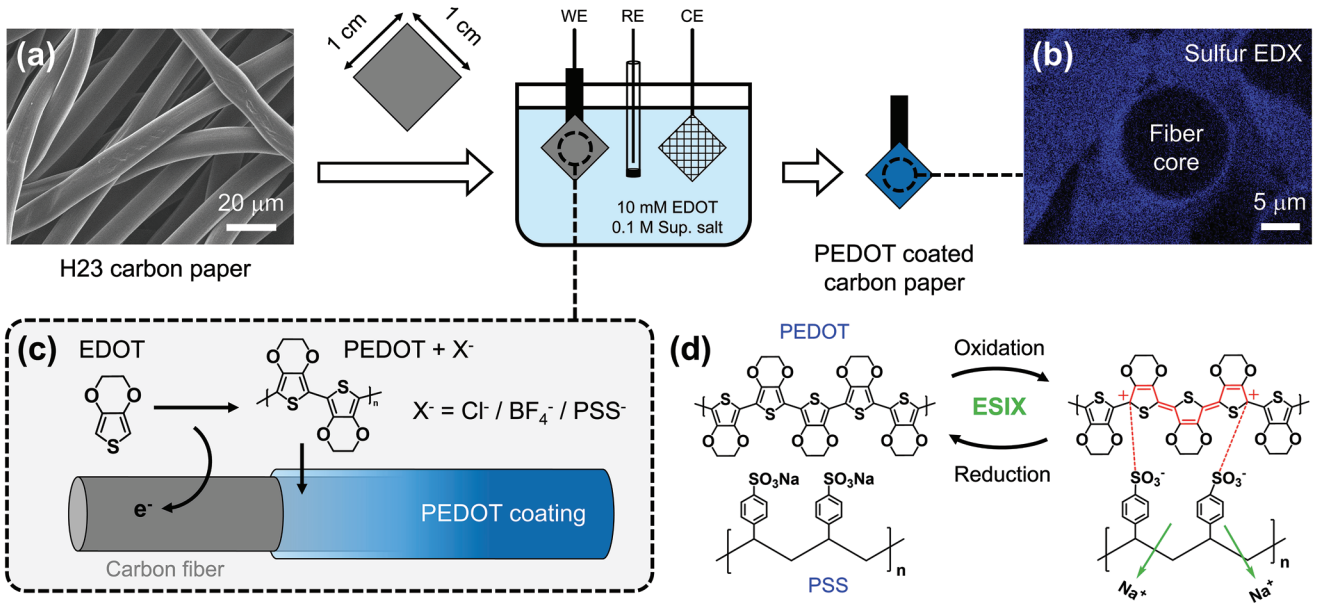

Scheme 1. Electropolymerization of PEDOT on carbon paper substrates. a) Carbon paper (Freudenberg H23) is cut in 1 cm^2 diamond shape and acts as a working electrode (WE) for the electropolymerization reactions. b) The resulting conformal coating can be seen via sulfur elemental map of a fiber cross section (contrast is adjusted for better visibility). c) Simplified reaction mechanism of EDOT electropolymerization on the fibers of carbon paper, where oxidation of EDOT causes it to dimerize and polymerize, resulting in its precipitation on the carbon surface. PEDOT takes up anions from the solution (provided by the supporting salt) during its electropolymerization, which are chlorine (Cl^-), tetrafluoroborate (BF_4^-) or PSS^- anions in this work. d) Illustration of the ESIX process of PEDOT/PSS. Upon oxidation, the positive charge of PEDOT is compensated by the adjacent sulfonate units of PSS^-, which forces the cations that used to coordinate to those sulfonate units (e.g., Na^+) to be expelled.

the electrochemical properties of PEDOT/PSS on carbon paper via cyclic voltammetry and showcase its ESIX capabilities by determining the loaded Ni^{2+}, Na^+, and Zn^{2+} amounts after electrosorption via elemental analysis. Finally, we determine the desorbed Ni^{2+} and Na^+ content after a full ESIX-swing via atomic absorption spectroscopy and correlate the separation efficiency to the coating thickness and weight. Through investigating the polymerization of PEDOT on porous scaffolds, we aim to connect the synthetic parameters to the coating morphology that is relevant for many electrochemical flow systems. We use selective separations as a platform to reveal the influence of coating thickness to an application specific metric that is ion-uptake capacity. We envision that the results from this work can guide the design of electropolymerization-based electrode coatings for various electrochemical technologies.

2. Experimental Section

2.1. Chemicals

3,4-Ethylenedioxythiophene (EDOT, 97%, Fluorochem), poly(sodium 4-styrenesulfonate) (PSSNa, 500–700 kDa, 20.4 wt%, Tosoh Organic Chemical Co.), potassium chloride (KCl, ≥99%, Merck), acetonitrile (MeCN, ≥99.9% HPLC grade, Merck), propylene carbonate (PC, anhydrous 99%, Merck), tetrabutylammonium tetrafluoroborate ($TBABF_4$, 99%, Fluorochem), nickel (II) sulfate hexahydrate ($NiSO_4 \cdot 6\ H_2O$, ≥99%, Merck), sodium sulfate (Na_2SO_4, ≥99%, Sigma Aldrich), potassium sulfate (K_2SO_4, ≥99%, Sigma Aldrich), zinc sulfate heptahydrate ($ZnSO_4 \cdot 7\ H_2O$, ≥99%, Sigma Aldrich) and nitric acid (HNO_3, 65%, VWR Chemicals) were used without further purification. All instances of water refer to ultrapure water (18.2 MΩ, ELGA PURELAB).

2.2. Substrates

Porous carbon electrodes (Freudenberg H23 carbon paper, 1 cm^2 geometric area, 210 µm nominal thickness, 80% porosity, FuelCellStore) were used as the electropolymerization substrates.[63] The morphology of PEDOT polymerized from aqueous solutions on pristine carbon paper is not conformal and the coating covers only the top surface of the substrate (see a comparison of coated substrates in Figures S1–S3, Supporting Information). Thus, to enhance the hydrophilicity of the porous electrode and ensure full wettability with the aqueous monomer solutions, carbon paper electrodes were also heat treated in a muffle oven with a heating ramp of 20 °C min^{-1} until 450 °C, kept at 450 °C for 12 h and naturally cooled down to room temperature.[64] Unless specified otherwise, aqueous electropolymerization was conducted on heat-treated carbon paper, while electropolymerization in organic solvents was conducted on pristine carbon paper.

2.3. Electropolymerization Setup

The electropolymerization substrates, Pt mesh (Pt, 99%, 2 cm diameter) and silver–silver chloride (BASi, Ag/AgCl in 3 M

KCl) or silver–silver ion electrodes (BASi, Ag/Ag^+) were used in a 3-electrode setup as the working, counter and the reference electrodes, respectively. Pt mesh was flame annealed before each experiment to remove organic contaminants. Ag/AgCl electrodes were used for aqueous solutions, whereas organic solvent-based solutions (MeCN and PC) utilized Ag/Ag^+ electrodes to avoid crystallization of KCl in the glass frit. Ag/Ag^+ electrodes were prepared before each experiment by immersing an Ag wire in 0.01 M $AgNO_3$ and 1 M $TBABF_4$ in MeCN or PC, depending on the solvent used in the experiment. The potentials of the Ag/Ag^+ electrodes versus the ferrocene/ferrocenium (Fc/Fc^+) couple can be found in Figure S4 (Supporting Information). The reactions were carried out in approximately 60 mL of the solutions filled in a glass electrochemistry cell (Metrohm AG). A depiction of the polymerization setup can be found in Scheme 1a. All samples were washed extensively with their respective solvents after electropolymerization to release weakly attached particles and unreacted monomers.

2.4. Electropolymerization of PEDOT

Aqueous electropolymerization of PEDOT was conducted with 0.01 M EDOT (as the monomer) and 0.1 M PSSNa or 0.1 M KCl (as the supporting salt) dissolved in water, and the resulting polymers are named as PEDOT/PSS or PEDOT/Cl, respectively. The molarity of PSSNa was calculated based on the molarity of the repeating unit (sodium 4-vinylbenzenesulfonate). Electropolymerization of PEDOT in organic solvents was conducted with 0.01 M EDOT (as the monomer) and 0.1 M $TBABF_4$ (as the supporting salt) dissolved in MeCN or PC, and the resulting polymers are named as PEDOT/BF_4-MeCN or PEDOT/BF_4-PC, respectively. All samples prepared in this work are tabulated in **Table 1** with their abbreviated names.

The substrates were coated under galvanostatic (constant current), potentiostatic (constant potential) or potentiodynamic (via cyclic voltammetry, CV) conditions with a potentiostat (Biologic VMP-300) in a 3-electrode setup. Constant current deposition of PEDOT/PSS coatings was carried out between 0.4 to 4 mA and 5 to 200 min; details can be found in the respective section of the manuscript. Constant current deposition of PEDOT/Cl, PEDOT/BF_4-MeCN and PEDOT/BF_4-PC coatings were carried out at 0.8 mA for 25 min, passing a total of 1.2 C charge. Constant potential deposition of all coatings was performed at 1 V versus their respective reference electrodes and terminated when 1.2 C was passed. CV deposition of all coatings was performed between –0.6 V to 1.3 V versus their respective reference electrodes at a scan rate of 100 mV s^{-1} and terminated when 1.2 C charge has passed. For potentiostatic and potentiodynamic conditions, automatic iR compensation was applied where the voltage was corrected with the solution resistance extracted at 100 kHz and 20 mV sinus amplitude at 85% compensation.

Table 1. Samples prepared in this work with their abbreviated names.

Sample name	Counterion	Solvent	Substrate
PEDOT/PSS	PSS^-	Water	Heat-treated carbon paper
PEDOT/Cl	Cl^-	Water	Heat-treated carbon paper
PEDOT/BF_4-MeCN	BF_4^-	Acetonitrile	Pristine carbon paper
PEDOT/BF_4-PC	BF_4^-	Propylene carbonate	Pristine carbon paper

2.5. Morphological Characterization and Thickness Extraction

The PEDOT coatings were examined with JEOL JSM IT-100 scanning electron microscope (SEM). The thickness of the PEDOT/PSS coatings was determined from a systematic analysis of SEM images with the DiameterJ plugin of the ImageJ software.[65] SEM images at 100× were segmented with the built-in script of DiameterJ and the image where only the topmost fibers are visible was picked as the best segmentation. Then, the script extracted the fiber thicknesses by measuring the visible fibers (approximately 50 fibers). An example procedure is depicted in Figure S5 (Supporting Information). Then, the measured fiber thicknesses were binned in a histogram and the mean fiber diameter was extracted with the standard error of the mean.The standard error of the mean was calculated as the pristine Freudenberg fibers have a large deviation in fiber diameter (±1 µm), causing the standard deviation of a submicron coating thickness to be unacceptably large. By utilizing a computer-assisted thickness extraction, we recorded approximately 50 000 thickness measurements over an area of 1.1 mm^2 on the samples. The resulting histograms of the two SEM images were averaged at different locations for each sample to reduce the effect of spatial variabilities in the coating thickness. In this way, the true mean of the fiber thickness can be closely estimated since the measurement population is very large. Uncoated fibers were measured with the same method and the coating thickness was determined by subtracting the coated fiber thickness from the uncoated fiber thickness and dividing by half. The standard errors were propagated accordingly.

2.6. Capacitance Measurements

The double-layer capacitance of the coated electrodes was measured using CV mode of the potentiostat in 0.1 M KCl without stirring. The potential was cycled from 0 to 0.4 V for 4 cycles at 5, 10, 20, 50 ,and 100 mV s^{-1} scan rates with automatic iR compensation. The current at 0.2 V for anodic and cathodic sweep of the last cycle was extracted and differential capacitance of cells was calculated by Equation 1:

$$i = \mathrm{EDLC}\frac{\mathrm{d}V}{\mathrm{d}t} \tag{1}$$

where i is the average current in absolute value [mA] at 0.2 V (vs Ag/AgCl), EDLC is the electric double-layer capacitance [F] and $\frac{\mathrm{d}V}{\mathrm{d}t}$ is the scan rate [mV s^{-1}]. The electrochemical surface area (ECSA) of the electrodes can then be calculated with Equation 2:

$$\mathrm{ECSA} = \frac{\mathrm{EDLC}}{C_{\mathrm{spec}}} \tag{2}$$

where ECSA is electrochemical surface area [m^2] and C_{spec} is the area-specific capacitance of carbon materials taken as 23 µF cm^{-2}.[64,66]

2.7. Electrosorption Experiments

All sorption experiments were conducted with a 3-electrode setup where PEDOT/PSS coated electrodes at different coating thicknesses were the working, Pt mesh was the counter and Ag/AgCl was the reference electrode. PEDOT/PSS coated electrodes with an area of 1 cm^2 were immersed in the electrolytes and a potential was applied with a potentiostat (Biologic VMP-300) using constant potential mode for 30 min. As solution conductivities may change over the course of an experiment, we opted out of compensating for the ohmic drop. Three potential values were applied where the sample is in the ESIX-inactive (electrodesorption), ESIX-active (electroadsorption) or electrodeposition regimes. Electrodeposition potentials can be calculated with the Nernst equation (Equation 3):

$$E_{red} = E^0 - \frac{RT}{nF} \ln Q \quad (3)$$

where E^0 is the standard reduction potential [V], R is the gas constant [J mol^{-1} K^{-1}], T is the temperature [K], n is the number of electrons transferred, F is the Faradays constant [C mol^{-1}] and Q is the reaction quotient. As the electrolyte, binary Ni-Na solutions contained 0.01 M $NiSO_4 \cdot 6\ H_2O$ with 0.1 M Na_2SO_4 and ternary Ni-Zn-Na solutions contained 0.01 M $NiSO_4 \cdot 6\ H_2O$, 0.01 M $ZnSO_4 \cdot 7\ H_2O$ and 0.1 M Na_2SO_4. The concentration of Na^+ was kept high to simulate real wastewater conditions. To prevent formation of ZnO, solutions with Zn^{2+} were acidified with nitric acid. The solutions were stagnant during the electrosorption reactions. After electrosorption of metals, now metal loaded PEDOT/PSS electrodes were extensively washed with ultrapure water and dried under air.

2.8. Analytical Techniques

The coating weight of PEDOT/PSS coated carbon paper samples was determined via the magnetic suspension balance of a gas sorption analyzer (Rubotherm IsoSORP SA). The coating amount was determined by subtracting the uncoated electrode weights from the weight of the coated and dried electrodes. This procedure was repeated on at least two separate sample sets and the standard deviations were calculated. The adsorption metrics were normalized with respect to coating mass and/or the coating thickness.

Metal loaded PEDOT/PSS electrodes were analyzed with energy-dispersive X-ray spectroscopy (EDX). EDX measurements were conducted with the detector housed within the SEM chamber, at 10 mm working distance and at 10 kV of accelerating voltage. The metal content of three separate samples (for binary adsorption experiments) or two separate samples (for ternary adsorption experiments) was measured via EDX and averaged to calculate the loaded metal amounts. The standard deviations were calculated accordingly.

Elemental measurements on the desorption solutions were conducted with a Shimadzu AA-7000 atomic absorption spectrophotometer (AAS) with air/acetylene flame and automatic background correction with a D_2 lamp for Ni signal. No background correction was necessary for Na signal. Adsorption calibration curves and fit parameters of Ni and Na can be found in Figure S6 and Table S1 (Supporting Information). Aliquots from desorption solutions were diluted to match the concentration range of the calibration curves. Each desorption experiment was performed once for each sample. The AAS signal was measured at least twice for each desorption solution and standard deviations are calculated. The error for weight normalized adsorption metrics was propagated by considering the standard deviation of the AAS measurements together with the standard deviation of the weight measurement. The complete sorption process is summarized below.

Conditioning: To condition the electrodes before the electrosorption procedure, PEDOT/PSS coated electrodes were immersed in 0.1 M HCl electrolyte and cycled between -0.6 V to 0.8 V (vs Ag/AgCl) at 50 mV s^{-1} via CV for 10 times and the last cycle ended at an oxidized state. By converting the sodiated PSS^- (PSSNa) into its acid form (PSSH), we tried to reduce the interference of residual Na on the AAS measurements.

Electroadsorption: Then, protonated PEDOT/PSS electrodes were immersed in the binary Ni-Na solutions with 0.01 M $NiSO_4 \cdot 6\ H_2O$ with 0.1 M Na_2SO_4 and a constant potential of –0.25 V (vs Ag/AgCl) was applied for 30 min.

Electrodesorption: For the desorption step, loaded electrodes were immersed in 0.05 M potassium sulfate solution and 0.6 V (vs Ag/AgCl) was applied for 30 min. The use of a salt ensures that the osmotic pressure is not dominant for the release of ions into the desorption solution, while the use of potassium sulfate ensures that the AAS measurements will not be compromised due to analyte or matrix effects.

3. Results and Discussion

3.1. Influence of Solvent, Counterion, and Electropolymerization Mode on PEDOT Coatings

PEDOT electropolymerized in the presence of counterions and these counterions are integrated into the structure as the resulting PEDOT oligomers are oxidized.[67] The size of these counterions not only influences the polymerization dynamics of PEDOT, but also determines the final ion-exchange properties of the coating. To study the influence of counterion size on the morphology, we polymerized PEDOT in the presence of PSS^- or Cl^- ions. PSS^- is a polyanion and is sterically hindered once it is incorporated within the polymer blend, while a small ion like Cl^- can move more freely.[57] Since both anions are highly soluble in water we utilized aqueous polymerization. PEDOT/PSS and PEDOT/Cl were polymerized using constant current, constant potential, or CV mode of the potentiostat and the resulting coatings are compared using SEM in **Figure 1**. PEDOT/PSS features a smooth surface at all polymerization modes and this could be caused by swelling of the PSS^- in the polymer layer. It is also possible that PSS^- solubilizes longer PEDOT oligomers and allows longer chains to be deposited, which causes a compact and dense coating to form.[68,69] It is not always apparent via microscopic investigation if there is a coating on the fibers when the coating is smooth. Thus, we also performed elemental mapping and verified that the PEDOT/PSS coatings are highly conformal and compact around the fibers (Figures S2 and S3, Supporting Information). There are also very few morphological

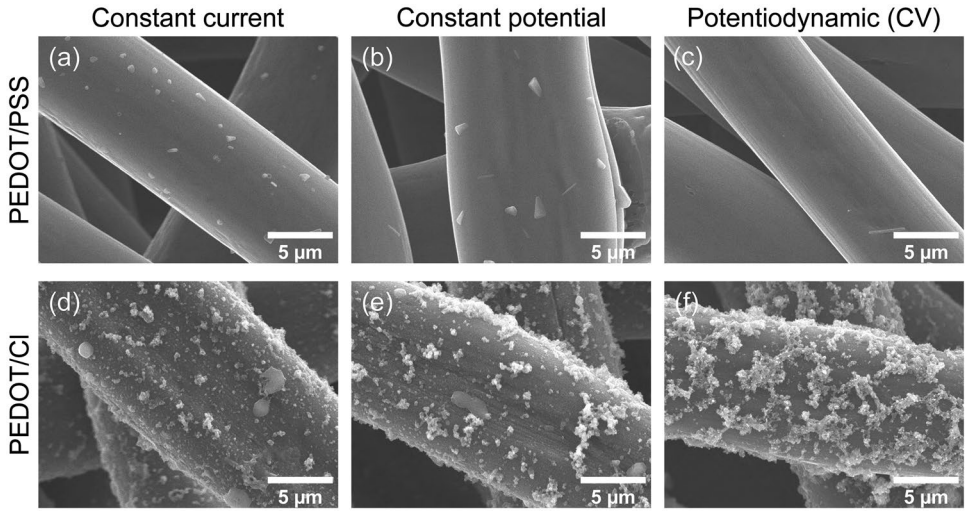

Figure 1. Influence of the counterion size on the morphology of aqueous PEDOT coatings on carbon paper. SEM pictures of a–c) PEDOT/PSS and d–f) PEDOT/Cl coated carbon papers at 5 KX magnification. The materials are polymerized using a,d) constant current, b,e) constant potential and c,f) CV modes. The reactions were terminated when 1.2 C of anodic charge have passed. Here, constant current polymerization conditions of PEDOT/PSS were identical to PEDOT/Cl. See Methods for further details on polymerization conditions.

differences between the polymerization modes for PEDOT/PSS (Figure 1a–c). PEDOT/Cl on the other hand has a powder-on-film morphology at all conditions (Figure 1d–f). These powdery structures tend to flake off from the fiber surface under mechanical deformation, which makes it difficult to handle the substrates and is not ideal for devices involving liquid flows. The polymerization conditions for PEDOT/Cl do impact the coating morphology, especially for potentiodynamic conditions where a rougher surface is visible (Figure 1f). Increased roughness when potential sweeps are employed together with the powder-on-film morphology hints at dissolution-redeposition processes during the polymerization of PEDOT/Cl coating.

The type of solvent determines the solubilities of reactants and products and influences the electric field within the electrolyte. As a consequence, the employed solvent strongly influences the final morphology of the conductive polymeric coatings.[60] The use of organic solvents, however, restricts the counterion space to supporting salts with lipophilic groups such as n-alkylammonium, PF_6^- or BF_4^-. Thus, we used acetonitrile (MeCN) and propylene carbonate (PC) as the solvents owing to their high dielectric constant and tetrabutylammonium tetrafluoroborate ($TBABF_4$) as the supporting salt. PEDOT/BF_4-MeCN and PEDOT/BF_4-PC were polymerized using constant current, constant potential or CV mode of the potentiostat and the resulting coatings were compared using SEM in **Figure 2**. The powder-on-film morphology is also observed in PEDOT/BF_4-MeCN in constant current mode, suggesting similar polymerization dynamics to PEDOT/Cl in water; however, the constant potential and CV modes deviate from this pattern as they feature a highly porous morphology with significant outgrowths. The solubility of the EDOT monomer and PEDOT oligomers are higher in organic solvents, which may accelerate the polymerization rate. In fact, in the case of PEDOT/BF_4-MeCN deposited using CV mode (Figure 2c), the substrate surface is completely covered with a highly porous layer that does not adhere to individual fibers. We attribute this to the combination of fast polymerization kinetics due to MeCN and the fast scan rate of the CV mode. The effect of solvent is even more dramatic in the case of PC as seen in the micrographs of PEDOT/BF_4-PC (Figure 2d–f). Only the constant current mode results in an adherent and compact coating on the fibers (Figure 2d). The potentiostatic condition (Figure 2e) has no material visibly deposited and we have not observed a sulfur signal on this sample via EDX. The potentiodynamic deposition in PC is also not optimal as the fiber is sparsely coated. It has been reported that PC is a better solvent for PEDOT oligomers than MeCN, which may result in diffusion of the products into the bulk electrolyte before they can precipitate on the fiber surface.[60] Indeed, we have observed significant colored product flowing under the carbon paper working electrode during the polymerization reactions in PC. Substrate–polymer incompatibility is unlikely as it is possible to coat the same polymer on carbon paper in MeCN. Although it is possible to coat PEDOT/BF_4 in PC on flat substrates, the difficult geometry of carbon paper excludes PC from being an ideal solvent for PEDOT electropolymerization for the conditions studied in this work.[60,70]

Based on these findings, we can infer that large counterions such as PSS^- dictate the morphology and reduce the influence of other synthetic parameters, whereas small counterions such as Cl^- and BF_4^- are more sensitive to the polymerization conditions and solubilities. However, if the solubility of the intermediates would be too high, there is a chance that the material will not properly deposit on the substrate, as observed in PC. Faster reaction kinetics (as in CV mode) causes smaller polymer segments and more open morphology to be generated. We revealed that PEDOT/Cl and PEDOT/BF_4-MeCN feature unstable outgrowths, rendering them unsuitable as coatings for porous electrodes that are intended to facilitate liquid flow. It is also clear that PC is not an ideal solvent for PEDOT polymerization on carbon paper. We conclude that PEDOT/PSS is the best candidate for electrochemical flow systems and continue investigating its properties.

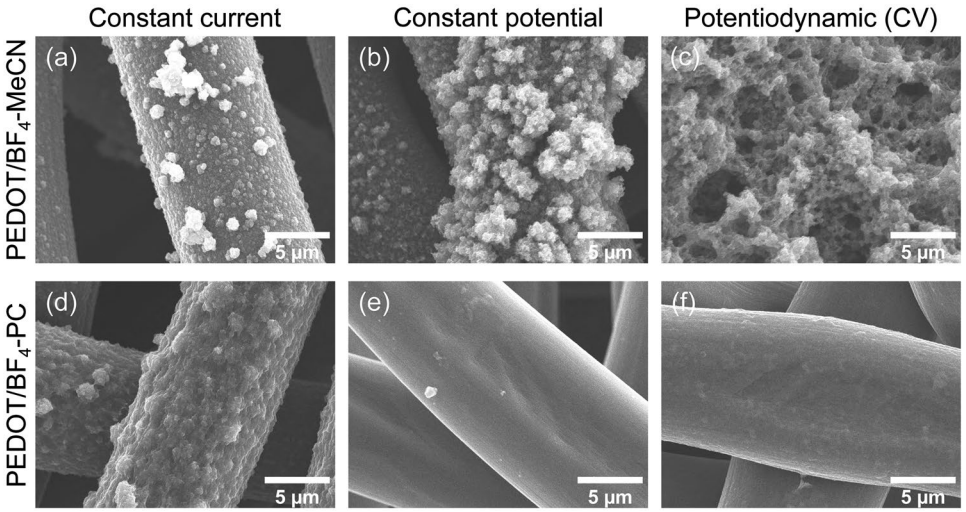

Figure 2. Influence of solvent on the morphology of PEDOT/BF_4 coatings on carbon paper. SEM pictures of a–c) PEDOT/BF_4-MeCN and d) PEDOT/BF_4-PC coated carbon papers at 5 KX magnification. Reaction at e) did not result in a coating. The materials are polymerized using a,d) constant current, b,e) constant potential, and c,f) CV modes. The reactions were terminated when 1.2 C of anodic charge have passed. See Experimental section for further details on polymerization conditions.

3.2. Morphology and Thickness of the PEDOT/PSS Coatings with Constant Current Polymerization

An inherent advantage of electrochemical synthetic techniques is that the amount of species reacted is related to the passed charge through Faraday's law. However, in the case of electropolymerization, the deposited amount is only a fraction of the species reacted due to the dissolution processes, side reactions, and charging of the oligomers and the polymer.[37] While controlling the deposited amount and correlating it to the coating thickness may be a straightforward task for flat substrates of known surface area, that is not the case for 3D structured materials such as fibrous electrodes. Having control over the coating thickness is important for flow applications as the fiber diameter influences the permeability of the porous scaffold. We also suspect coating thickness to play a role in the species transport during ESIX processes as species must be ingressed and expelled across the coated layer. The ion uptake mechanism for conductive polymers is not only on the surface, but also through the bulk, which can result in underutilization of the coating as ion diffusion is not fast (relative to the solution) within the bulk of the material.[71,72] As the active material gets thicker on the porous electrode, slow ion adsorption may hinder the separation process. Thus, the coating thickness must be precisely controlled to maximize the mass transport benefits of a porous scaffold while not hindering the ion exchange. Considering these points, we investigated the layer thickness of PEDOT/PSS on carbon paper as a function of current and polymerization time using constant current operation.

First, we kept the time as a constant (25 min), but varied the current value (see Figure S7, Supporting Information for the chronopotentiograms). In this way, we can investigate the influence of current on the layer thickness and the morphology. We extracted the fiber thicknesses from the micrographs via a systematic analysis (see Experimental section–Characterization). The resulting histograms of the measured fiber thicknesses for the increasing current experiment can be found in **Figure 3**a. After extracting the fiber thicknesses from bare and coated fibers, we can calculate the coating thickness. The measured coating thicknesses of the increasing current experiment (Figure 3b) reveal that higher currents result in thicker coatings up to a certain current. The skewed thickness values can be fit with a log-normal distribution function, representing the decreasing efficiency of the polymerization reaction as the current increases. There is a limit on the current that can be realized as side reactions can dominate over EDOT oxidation, especially when the potential exceeds the solvent stability window. This is supported by the observed carbon corrosion at 4 mA (see Figure 3c). In this case, high current demand from the carbon paper support may have resulted in an extreme case of side reaction.[73,74] We postulate that gas bubbles could be trapped in these areas which prevented liquid contact and caused local reactant starvation. The heat treatment of the substrate should reduce the occurrence of such events, but it cannot eliminate it completely due to the inherent hydrophobicity of the porous substrate. At more moderate currents we do not observe such major defects (Figure 3c).

Then, we fixed the current at a constant value (0.4 mA) and varied the time to control the passed charge (see Figure S8, Supporting Information for the chronopotentiograms). Using this approach, we keep the reaction rate similar between experiments. We opted for this lower current value as it has least amount of visible imperfections, though the current can be safely increased to 2 mA and a high-quality coating can be reached. For the increasing time experiment, the rate of growth in thickness is decreasing (**Figure 4**b). This is in contrast to linear trends observed for such coatings before.[62] However, this is an expected trend for a fibrous substrate since there is a square-root scaling between the volume and thickness of a hollow cylinder. Indeed, fitting the coating thickness versus coating time (an approximation of coating volume through Faraday's law) plot to a square-root function is possible with R^2 close to 1. This makes reaching a targeted coating thickness

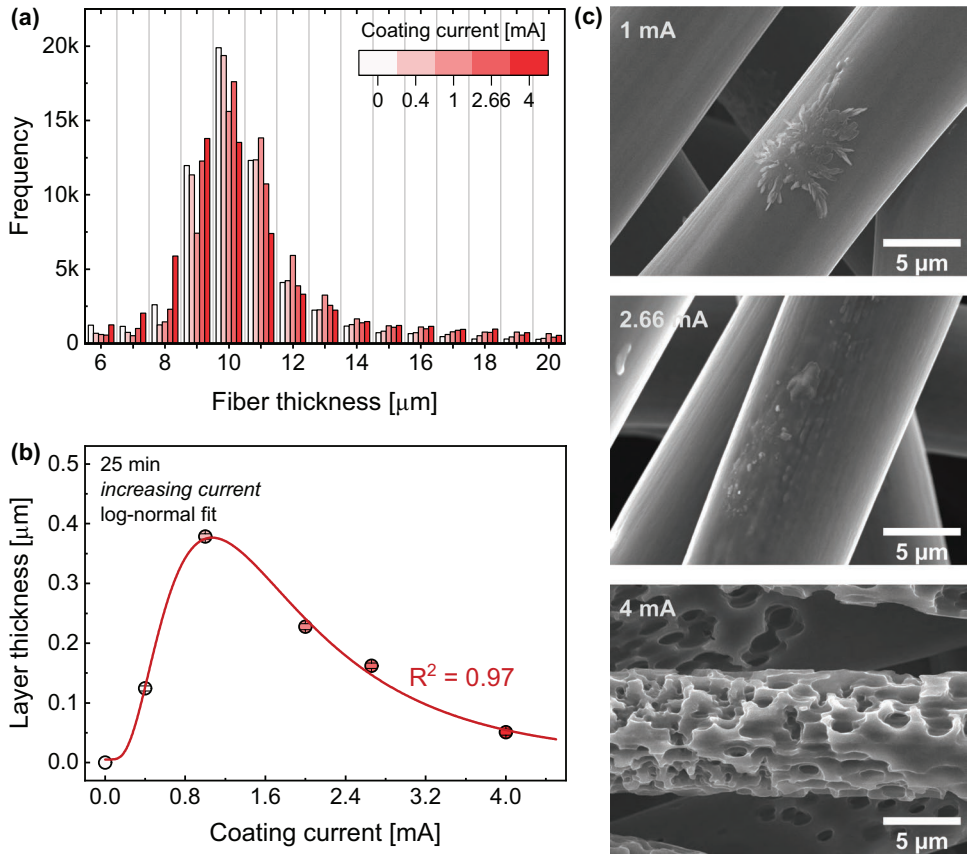

Figure 3. Thickness and morphology of PEDOT/PSS coatings polymerized for 25 min at increasing coating currents. a) Averaged histograms of measured fiber thicknesses for PEDOT/PSS coated carbon paper at various current values. b) Mean layer thicknesses extracted from the histogram plotted as a function of coating current. c) Micrographs at 5 KX magnification of PEDOT/PSS coated carbon paper with increasing current protocol at 1, 2.66, and 4 mA.

easier, at the expense of longer operation times for thicker coatings. From a morphological perspective, all samples are coated with a thin layer of PEDOT/PSS and the coating is visibly smooth until the 100 min coating time, where roughness starts to appear (Figure 4c). We also collected EDX spectra at various locations for thin coatings to make sure that a PEDOT/PSS layer exists on the fiber (see Figure S9 in the Supporting Information). There is a straightforward relation between the coating thickness and the coating time for the increasing time experiment, thus we recommend current to be fixed at a moderate-to-low value for PEDOT/PSS polymerization if thickness control is a factor.

3.3. Electrochemical Properties of the PEDOT/PSS Coatings

Unlike redox-active polymers with pendant active groups where a distinct redox event can be observed, the redox response of conductive polymers is usually complex. Upon oxidation of PEDOT/PSS, the positive charge is delocalized on the polythiophene backbone in the form of polarons and bipolarons which span multiple thiophene rings.[75] Having multielectron transfer processes, variability in the conjugated chain length, and increased capacitance during charging influence the oxidation potential of the polymer, further complicating the analysis. As seen in **Figure 5**a, the voltammogram of PEDOT/PSS coated carbon paper does not show distinct redox peaks. Instead, the material demonstrates a pseudocapacitive response. This voltage-dependent capacitance of PEDOT/PSS is in fact a property of its redox activity and can be utilized in the ESIX processes. It is not easy to distinguish at which potential PEDOT starts to get oxidized from the voltammogram, but we expect the onset of oxidation to be around 0 V versus Ag/AgCl and continue until 0.8 V based on existing literature.[76] This potential will be assumed as the onset of redox-switching potential of PEDOT for the rest of this study.

The capacitance of the coatings can be extracted from CV curves at various scan rates (Figure S10, Supporting Information), the resulting graphs can be seen in Figure 5b. PEDOT/PSS coated carbon paper demonstrates a larger capacitance than the uncoated carbon paper (Figure 5b), which is expected as the PEDOT/PSS coating is electroactive and is a pseudocapacitive material. We observed higher capacitance for PEDOT/Cl coatings compared to PEDOT/PSS, which could be due to its rougher morphology, resulting in a larger surface area, and we expect even higher capacitance from PEDOT/BF_4-MeCN coatings owing to their highly porous structure. Although double-layer capacitance is an important mechanism for electroadsorption of ions, it is not inherently selective towards anions or cations, let alone different types of cations. The ESIX

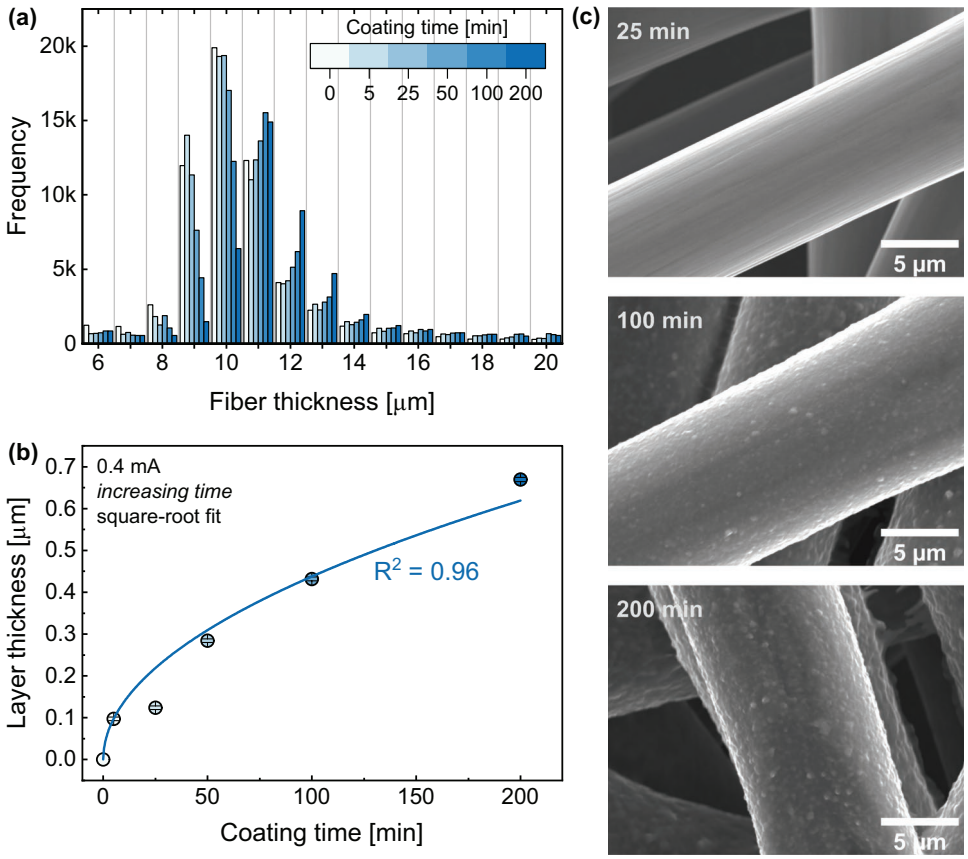

Figure 4. Thickness and morphology of PEDOT/PSS coatings polymerized at 0.4 mA with increasing coating time. a) Averaged histograms of measured fiber thicknesses for PEDOT/PSS coated carbon paper for various coating times. b) Mean layer thicknesses extracted from the histogram plotted as a function of coating time. c) Micrographs at 5 KX magnification of PEDOT/PSS coated carbon paper with increasing time protocol for 25, 100, and 200 min.

mechanism builds up on the double layer by extending the adsorption into the bulk of the electroactive material. However, it is not possible to reveal the ESIX property of PEDOT/PSS coatings with conventional electrochemical techniques such as capacitance measurements. Thus, we used spectroscopic techniques to reveal the metal loading on coated substrates and studied the affinity of the polymer system toward different cations.

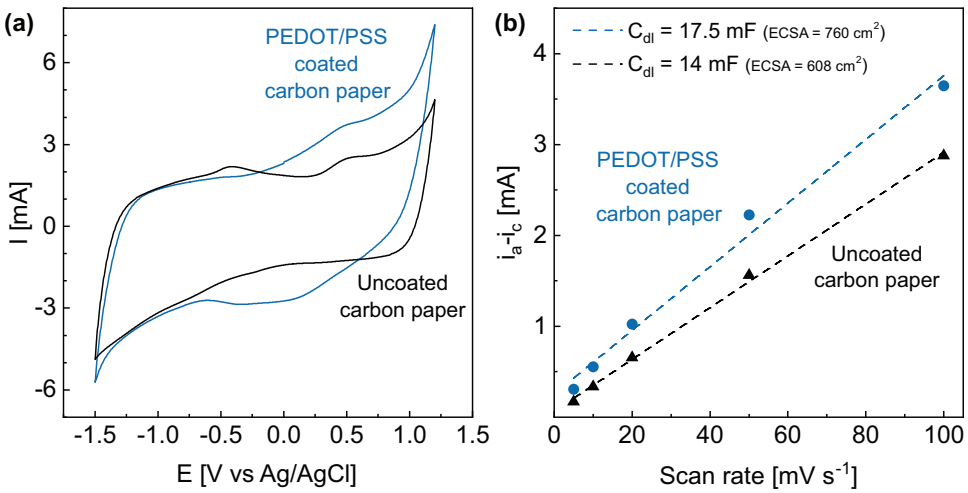

Figure 5. Electrochemical characterization of PEDOT/PSS coated carbon paper. a) Cyclic voltammogram and b) capacitance of the PEDOT/PSS coated and uncoated carbon papers. CV is recorded at 100 mV s^{-1} and both experiments are conducted in 0.1 M KCl with automatic iR compensation.

ADVANCED MATERIALS INTERFACES
Open Access
www.advmatinterfaces.de

3.4. Demonstration of the ESIX Property of PEDOT/PSS Coated Carbon Papers

Although the capacitance of the coated substrates is higher than that of the uncoated carbon paper, it is the redox-switching property of PEDOT that is useful in the electrochemically switched ion exchange process. The ion exchange in ESIX materials occurs based on a Faradaic potential switch rather than the double-layer charging process.[21] The possibility to electrochemically oxidize the conductive polymer backbone enables the ion-exchange process to be controlled by an applied potential. Since ions can be separated when the redox reactions of the polymer take place, lower potentials can be applied to the system compared to electrodeposition-based and capacitive methods.[12,20]

To demonstrate the ESIX activity of the PEDOT/PSS coated carbon paper, we chose to perform Ni^{2+} separation as it is an environmental pollutant with significant cytotoxicity, and an excess of Na^+ is used to simulate wastewater conditions.[77] Zn^{2+} is another transition metal that is found in high quantities together with Ni^{2+} in electroplating wastewater and thus is employed to probe the selectivity of the PEDOT/PSS system.[78] The substrates were PEDOT/PSS coated carbon papers at two coating times (25 min and 100 min) that were polymerized via constant current operation at 0.4 mA. We opted for 0.4 mA for the coatings to ensure minimal defects on the polymer layer and because the coating thicknesses have been determined previously (Figure 3).

To perform ESIX, we must ensure that electrodeposition reactions do not take place on the electrode, while making sure PEDOT is reduced to a sufficient degree. The reduction potentials of the transition metal ions in this study (E^{red}_{metal}, metal = Ni^{2+}, Zn^{2+}) are adjusted based on the experimental conditions according to Equation 3, and are –0.5 V for Ni^{2+} and –1 V for Zn^{2+} (vs Ag/AgCl). Along with the redox onset of PEDOT/PSS around 0 V, the redox potentials encountered in this system naturally create three potential regimes (**Figure 6**a). These are ESIX-inactive ($E^{applied} > 0$ V), ESIX-active ($0 V > E^{applied} > E^{red}_{metal}$) and electrodeposition ($E^{applied} < E^{red}_{metal}$) regimes. The ESIX-active regime is where the electrosorption reactions take place and is higher in potential than the electrodeposition potential of the metal being used, which should result in ion uptake within the polymer without reduction of the metal ion itself. To verify this hypothesis, we applied the same procedure to the uncoated heat-treated carbon paper, which should not demonstrate any ESIX capabilities. Thus, we have applied three potentials on the coated and bare substrates, in binary solutions with Ni^{2+} (0.01 M) and Na^+ (0.2 M), and in ternary solutions of Ni^{2+} (0.01 M), Zn^{2+} (0.01 M) and Na^+ (0.2 M). We determined the loaded metal amounts via EDX (see Experimental section—Analytical techniques) after a set potential is applied for 30 min (Figure 6b).

In both electrolytes, PEDOT/PSS coated electrodes take up a certain amount of metal irrespective of the applied potential. This is expected, as during polymerization, the PSS^- segments that neutralize oxidized PEDOT oligomers will carry the whole

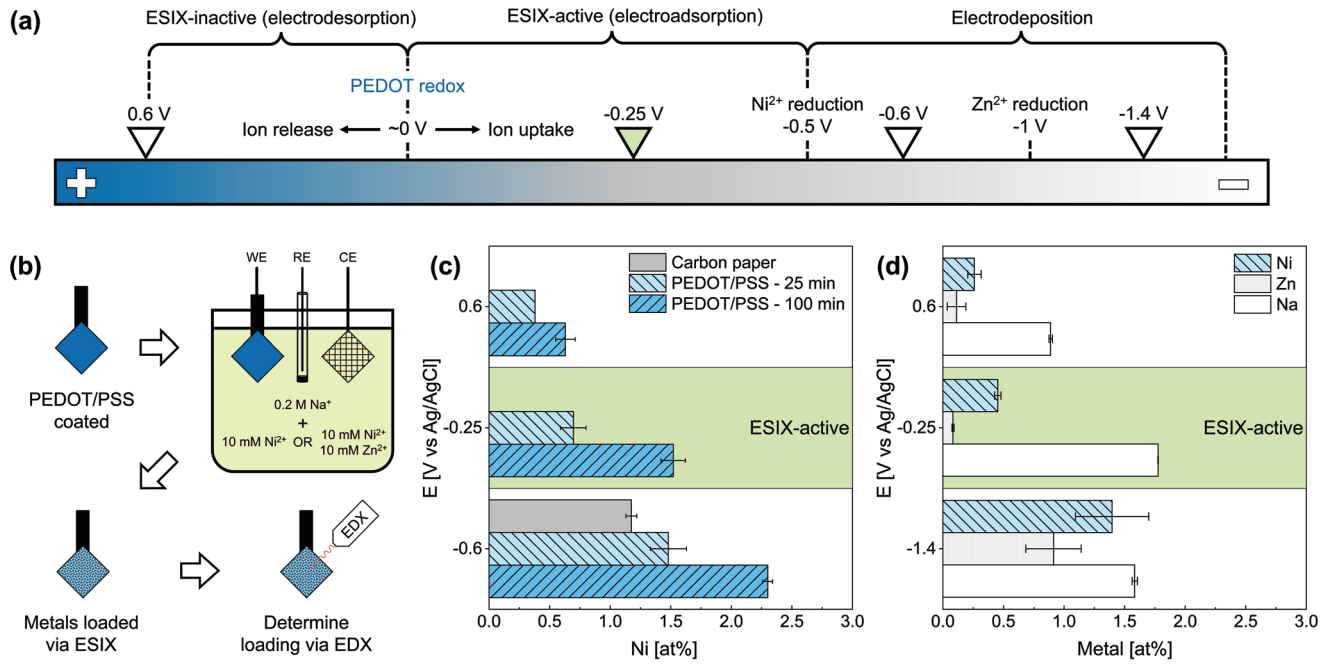

Figure 6. ESIX process on PEDOT/PSS coated carbon papers demonstrated with metal cations. a) Schematic depiction of the potential scale for the ESIX experiments with the relevant redox potentials and applied potentials. b) Scheme of electroadsorption of metal ions on PEDOT/PSS coated carbon paper. The loaded metal amounts are determined via EDX. c) Adsorbed or electrodeposited Ni amounts on uncoated and PEDOT/PSS coated carbon papers (polymerized for 25 min and 100 min at 0.4 mA) after applying various potentials in binary Ni–Na electrolytes. d) Adsorbed or electrodeposited metal amounts on uncoated and PEDOT/PSS coated carbon papers (polymerized for 25 min at 0.4 mA) after applying various potentials in ternary Ni–Zn–Na electrolytes. Error bars represent standard error of the mean for three separate samples for binary and two samples for ternary electrolyte adsorption experiments.

PSS^- chain into the blend structure, which results in an excess of styrene sulfonate units (compared to the positive charges of the PEDOT).[79] Consequently, the PSS^- segments that are not compensating for the positive charge of the PEDOT chains do not respond to the redox reactions of PEDOT. The ions associated with these units cannot be exchanged via ESIX and are subjected to conventional ion exchange.[80] Thus, we can observe Ni and Zn at 0.6 V for thin and thick coatings (Figure 6c,d), which would not be the case if electroadsorption was the only process.

In Figure 6c, we observe that the thicker PEDOT/PSS coating (0.43 µm based on Figure 3) takes up more Ni^{2+} than the thinner PEDOT/PSS coating (0.12 µm based on Figure 3) at all potential regimes, which can be explained by the existence of more ion adsorption sites in a thicker coating. Interestingly, the Ni^{2+} amounts normalized to layer thickness $\left(\frac{\text{adsorbed Ni at\%}}{\text{Thickness}_{\text{PEDOT/PSS}}}\right)$ are larger for thinner coating (5.79 at% Ni^{2+} μm^{-1}) than the thicker one (3.53 at% Ni^{2+} μm^{-1}), which suggests that the polymer layer has mass transfer limitations for ion-uptake. More importantly, the loaded Ni^{2+} amount nearly doubles when the potential is switched from 0.6 to -0.25 V for both coatings. This potential switch forces the oxidized PEDOT segments to reduce into a neutral state, which triggers the PSS units to ingress cations from the solution to compensate its negative charge. Thus, the increased EDX signal is a strong indication that the system has switched into an ESIX-active state and consequently took up ions from the solution. Furthermore, it is not possible for the uncoated carbon paper to take up cations unless electrodeposition process takes place. This highlights the energy efficiency of ESIX process for wastewaters with low metal concentrations since depositing metals from dilute solutions require significant overpotentials.

In Figure 6d, we observe the ion uptake of thinner PEDOT/PSS (polymerized for 25 min at 0.4 mA, 0.2 µm based on Figure 3) from ternary solutions of Ni^{2+}, Zn^{2+}, and Na^+. In all potential regimes, Ni^{2+} adsorption is higher compared to Zn^{2+}, which can be explained by the smaller hydrodynamic radius of Ni^{2+} (404 pm) than Zn^{2+} (430 pm).[81] It has been reported before that the cation selectivity of a similar poly(pyrrole)/PSS system is determined by PSS^- and the conductive polymer only acts as a switching matrix.[82] Although the hydrodynamic radius of Na^+ (358 pm) is smaller than both Ni^{2+} and Zn^{2+}, it is a monovalent cation and ion valence plays a bigger role in the selectivity of PSS.[83] We expect a similar behavior from electropolymerized PEDOT/PSS layers, thus ions with a higher valence (Ni^{2+} vs Na^+) and of smaller hydrodynamic radius (Ni^{2+} vs Zn^{2+}) should have a higher affinity towards PEDOT/PSS. At all potentials, the system took up Na^+ ions with a higher loading than other cations, which is partly because of its 20-times higher concentration in the adsorption solutions and partly because there is residual sodium in the polymer structure due to the use of the sodium salt of poly(4-styrenesulfonate). Due to these limitations, although useful to showcase the ESIX concept, EDX analysis can only provide semiquantitative information on the metal loading. We also observe that the presence of Zn^{2+} in the electrolyte significantly decreases the Ni^{2+} affinity (over Na^+) within the ESIX regime. The electroadsorption of metals on the coated electrodes provides important information on the ESIX process on porous systems, but it is possible to move one step further in the mechanism by considering the electrodesorption of ions. Thus, we next investigate the separation performance of PEDOT/PSS with AAS measurements on desorption solutions for Ni and Na.

3.5. Complete ESIX Swing of PEDOT/PSS Coated Carbon Papers for Ni Separation

We have demonstrated that PEDOT/PSS coated carbon paper electrodes can faradaically capture cations from solutions via the ESIX process. Loaded metal amounts on thin and thick coatings as determined by EDX suggest that thinner coatings are better utilized for metal loading via ESIX and this can influence the release of cations as well. To compare the effect of thickness and polymer weight on the cation desorption kinetics, we polymerized PEDOT/PSS for increasing polymerization times. Following the same experimental procedure that resulted in the layer thicknesses of Figure 3 (0.4 mA for 25, 50, 100 and 200 min), the carbon paper electrodes were coated with PEDOT/PSS with increasing polymer weights (**Table 2**). The details of the complete ESIX swing can be found in the Material and Methods. Briefly, the electrodes were first electrochemically cycled in an acid solution (0.1 M HCl) to protonate the PSSNa and reduce the influence of residual sodium on the measurements. Then, electroadsorption in binary Ni-Na solutions took place, as described in the previous section. Finally, the electrodes were placed in a K_2SO_4 solution and 0.6 V was applied for 30 min. This potential corresponds to an oxidized region of PEDOT, which should release cations from the polymer layer via electrodesorption. We took aliquots from the desorption solutions and determined the metal content after dilutions via AAS (**Figure 7**a).

We find that the uptake capacity for both ions increases with increasing polymerization time (Figure 7b), which is expected as a thicker coating should have more adsorption sites. The Na^+ uptake does not increase at the same rate as Ni^{+2}, highlighting the affinity of the system towards divalent cations. This shows that it is possible to separate Ni^{2+} from excess Na^+ via full ESIX swing of the PEDOT/PSS coated carbon paper. The desorbed Ni amount can be normalized with respect to the amount of PEDOT/PSS to find the adsorption capacity (Figure 7c), which can be compared with similar material systems (Table S2 in Supporting Information). The adsorption capacity decreases with increasing thickness, which is in line with previous observations. Thinner coatings with less mass are better utilized within the time frame of the ESIX

Table 2. Coating weights of PEDOT/PSS on carbon paper, determined via magnetic suspension balance. The errors are standard deviations of at least 2 separate samples from the mean.

Polymerization time	Current [mA]	Passed charge [C]	Coating weight [mg]
25 min	0.4	0.6	0.25 ± 0.007
50 min	0.4	1.2	0.65 ± 0.02
100 min	0.4	2.4	1.54 ± 0.06
200 min	0.4	4.8	3.27 ± 0.1

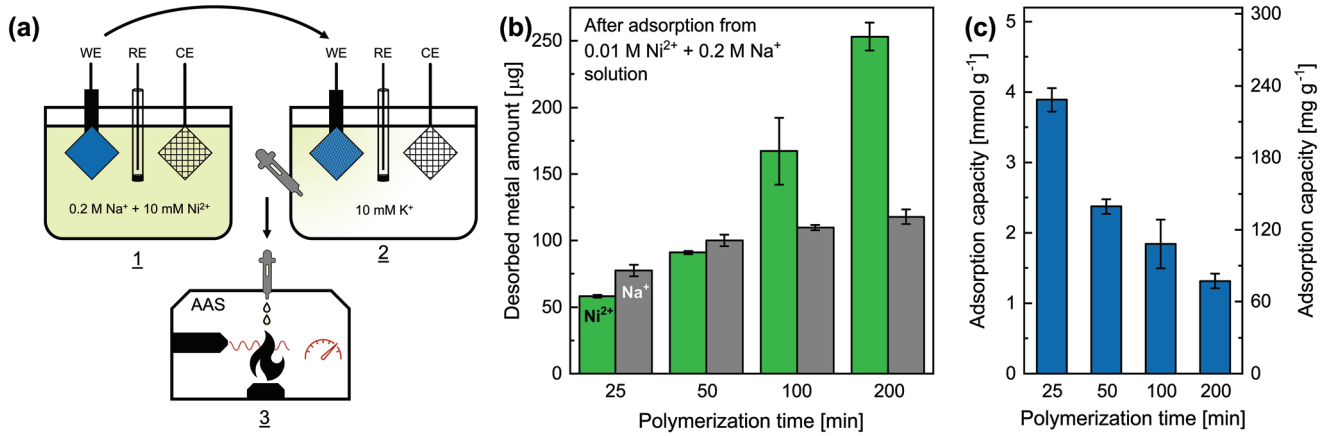

Figure 7. Desorption of Ni and Na from PEDOT/PSS coated carbon paper via ESIX. a) Schematic of the ESIX-swing where electroadsorption (1) is followed by electrodesorption (2) and the desorbate it analyzed via AAS (3). b) Desorbed Ni and Na amounts from PEDOT/PSS on carbon paper as determined by AAS measurements on samples with increasing coating times. The error bars represent the standard deviation of the AAS signal for each sample. c) Adsorption capacity of PEDOT/PSS for Ni normalized against the coating weights, as a function of polymerization time. The error bars are standard deviations propagated from the deviation of the AAS signal with the deviation of the sample weights.

experiments, suggesting that mass transfer limitations within the active material are a dominant factor in ESIX-based ionic separations. It has been reported that cations can be trapped in the polymer layer during the cycling of a similar PEDOT/sodium dodecylsulfate blend system.[57] Thus, the larger size of Ni^{2+} (than Na^{+}) may have prevented its efficient removal during desorption. It is worth noting that the current plateau is reached early within the experiment time frame in chronoamperograms of electroadsorption and electrodesorption experiments (Figure S11a, Supporting Information). Samples with a longer polymerization time have more coating mass, but a lower mass utilization and the maximum capacity of 3.8 mmol g^{-1} (228 mg g^{-1}) for Ni is reached for the coating with 25 min of polymerization time.

In this study, we investigated the adsorption capabilities of electropolymerized coatings of PEDOT/PSS on porous carbon paper substrates in three-electrode cells with stagnant solutions. We envision that industrial-scale ionic separations would be conducted in two electrode setups, with stacks of electrodes under hydrodynamic conditions. The flowing electrolyte could decrease the mass transfer limitations observed in this study and allow the maximum adsorption capacity of the coating to be reached at a shorter time.

4. Conclusions

In this work, we have studied electropolymerization of PEDOT onto porous carbon paper electrodes for its application in electrochemical flow systems, with a focus on ionic separations. We investigated the influence of the electrochemical protocol, counterion, and solvent choice on the morphology of the resulting PEDOT coatings. We revealed that large counterions such as PSS^{-} determine the morphology, while small counterions such as Cl^{-} and BF_4^{-} are more susceptible to the electrochemical protocol and solvent choice. PEDOT/PSS blend structure proved to be the best choice from a coating stability perspective and due to its smoothness and insensitivity to synthetic parameters. For PEDOT/PSS coatings, we have observed that higher currents induce thicker coatings on the fibers of the porous mat, but are susceptible to cause side reactions, while a low (but steady) current allows reaching a thickness down to 0.1 µm in a controllable fashion. Finally, we showcased the use of PEDOT/PSS coated carbon papers for ESIX-based separation of transition metals and found out that the coated electrodes have higher affinity for Ni^{2+} than Zn^{2+} and Na^{+}. By analyzing the metal amounts in desorption solutions after a full ESIX swing, we revealed that maximum Ni adsorption capacity for the PEDOT/PSS coatings is 3.8 mmol g^{-1} in terms of coating weight. The emerging electrochemical flow systems for energy and environmental applications can benefit greatly from porous electrodes with coatings where functionality and conformality are simultaneously desired. Thus, we hope that this work will inform researchers into methods and parameters on how to apply a functional coating on porous electrodes in a conformal fashion and how physical properties of thin polymer coatings influence their ion-exchange performance.

Supporting Information

Supporting Information is available from the Wiley Online Library or from the author.

Acknowledgements

E.B.B. and A.F.-C. gratefully acknowledge funding from the Eindhoven Institute of Renewable Energy System (EIRES). The authors would like to thank Kitty Nijmeijer (Eindhoven University of Technology) for her mentorship and feedback on the manuscript.

Conflict of Interest

The authors declare no conflict of interest.

Author Contributions

E.B.B. contributed to the conceptualization, methodology, formal analysis, investigation, data curation, writing-original draft, writing, review and editing, and visualization, M.F. contributed to methodology, formal analysis, investigation and data curation. Finally, A.F.-C. contributed to the conceptualization, methodology, funding, resources, writing-original draft, writing-review and editing, project administration, and supervision.

Data Availability Statement

The data that support the findings of this study are available from the corresponding author upon reasonable request.

Keywords

conducting polymers, electrochemical separations, electropolymerization, ESIX, PEDOT, porous carbon electrodes

Received: December 22, 2022
Revised: January 27, 2023
Published online: March 2, 2023

[1] International Energy Agency, Energy Technology Perspectives 2020, OECD **2020**, https://doi.org/10.1787/d07136f0-en.
[2] T. Watari, K. Nansai, K. Nakajima, *Resour., Conserv. Recycl.* **2020**, *155*, 104669.
[3] I. Directorate-General for Internal Market, S. Bobba, S. Carrara, J. Huisman, F. Mathieux, C. Pavel, *Critical Raw Materials for Strategic Technologies and Sectors in the EU: A Foresight Study*, Publications Office Of The European Union, LU **2020**, https://data.europa.eu/doi/10.2873/58081.
[4] M. Miranda, P. Burris, J. F. Bingcang, P. Shearman, J. O. Briones, A. La Viña, S. Menard, *Mining and Critical Ecosystems: Mapping the Risks*, World Resources Institute, Washington, DC **2003**, https://files.wri.org/d8/s3fs-public/pdf/mining_critical_ecosystems_full.pdf.
[5] Q. Zhou, N. Yang, Y. Li, B. Ren, X. Ding, H. Bian, X. Yao, *Global Ecol. Conserv.* **2020**, *22*, e00925.
[6] M. T. Bankole, A. S. Abdulkareem, I. A. Mohammed, S. S. Ochigbo, J. O. Tijani, O. K. Abubakre, W. D. Roos, *Sci. Rep.* **2019**, *9*, 4475.
[7] K. Kim, R. Candeago, G. Rim, D. Raymond, A.-H. A. Park, X. Su, *iScience* **2021**, *24*, 102374.
[8] X. Su, *Electrochem. Soc. Interface* **2020**, *29*, 55.
[9] A. Kumar, G. Naidu, H. Fukuda, F. Du, S. Vigneswaran, E. Drioli, J. H. Lienhard, *ACS Sustainable Chem. Eng.* **2021**, *9*, 7704.
[10] M. A. Alkhadra, X. Su, M. E. Suss, H. Tian, E. N. Guyes, A. N. Shocron, K. M. Conforti, J. P. de Souza, N. Kim, M. Tedesco, K. Khoiruddin, I. G. Wenten, J. G. Santiago, T. A. Hatton, M. Z. Bazant, *Chem. Rev.* **2022**, *122*, 13547
[11] P. Srimuk, X. Su, J. Yoon, D. Aurbach, V. Presser, *Nat. Rev. Mater.* **2020**, *5*, 517.
[12] X. Su, *Curr. Opin. Colloid Interface Sci.* **2020**, *46*, 77.
[13] Y. Oren, *Desalination* **2008**, *228*, 10.
[14] R. Chen, T. Sheehan, J. L. Ng, M. Brucks, X. Su, *Environ. Sci.* **2020**, *6*, 258.
[15] J. Lee, S. Kim, C. Kim, J. Yoon, *Energy Environ. Sci.* **2014**, *7*, 3683.
[16] S. Zavahir, T. Elmakki, M. Gulied, Z. Ahmad, L. Al-Sulaiti, H. K. Shon, Y. Chen, H. Park, B. Batchelor, D. S. Han, *Desalination* **2021**, *500*, 114883.
[17] M. Pasta, A. Battistel, F. L. Mantia, *Energy Environ. Sci.* **2012**, *5*, 9487.
[18] C. P. Lawagon, G. M. Nisola, R. A. I. Cuevas, H. Kim, S.-P. Lee, W.-J. Chung, *Chem. Eng. J.* **2018**, *348*, 1000.
[19] T. Kim, C. A. Gorski, B. E. Logan, *Environ. Sci. Technol. Lett.* **2017**, *4*, 444.
[20] S. Porada, A. Shrivastava, P. Bukowska, P. M. Biesheuvel, K. C. Smith, *Electrochim. Acta* **2017**, *255*, 369.
[21] M. A. Lilga, R. J. Orth, J. P. H. Sukamto, S. M. Haight, D. T. Schwartz, *Sep. Purif. Technol.* **1997**, *11*, 147.
[22] X. Hao, Y. Li, M. Pritzker, *Sep. Purif. Technol.* **2008**, *63*, 407.
[23] K. Nakahara, K. Oyaizu, H. Nishide, *Chem. Lett.* **2011**, *40*, 222.
[24] J. Roncali, *Chem. Rev.* **1992**, *92*, 711.
[25] R. Pietschnig, *Chem. Soc. Rev.* **2016**, *45*, 5216.
[26] U. S. Schubert, C. Eschbaumer, *Angew. Chem., Int. Ed.* **2002**, *41*, 2892.
[27] X. Su, K.-J. Tan, J. Elbert, C. Rüttiger, M. Gallei, T. F. Jamison, T. A. Hatton, *Energy Environ. Sci.* **2017**, *10*, 1272.
[28] X. Su, A. Kushima, C. Halliday, J. Zhou, J. Li, T. A. Hatton, *Nat. Commun.* **2018**, *9*, 4701.
[29] E. R. Reale, A. Shrivastava, K. C. Smith, *Water Res.* **2019**, *165*, 114995.
[30] X. Du, X. Hao, Z. Wang, G. Guan, *J. Mater. Chem. A* **2016**, *4*, 6236.
[31] T. F. Baumann, M. A. Worsley, T. Y.-J. Han, J. H. Satcher, *J. Non-Cryst. Solids* **2008**, *354*, 3513.
[32] Y. Liu, Y. Zhang, Y. Zhang, Q. Zhang, X. Gao, X. Dou, H. Zhu, X. Yuan, L. Pan, *J. Mater. Chem. A* **2020**, *8*, 1443.
[33] W. Tang, J. Liang, D. He, J. Gong, L. Tang, Z. Liu, D. Wang, G. Zeng, *Water Res.* **2019**, *150*, 225.
[34] K. J. Kim, M.-S. Park, Y.-J. Kim, J. H. Kim, S. X. Dou, M. Skyllas-Kazacos, *J. Mater. Chem. A* **2015**, *3*, 16913.
[35] L. Cindrella, A. M. Kannan, J. F. Lin, K. Saminathan, Y. Ho, C. W. Lin, J. Wertz, *J. Power Sources* **2009**, *194*, 146.
[36] M. Son, V. Pothanamkandathil, W. Yang, J. S. Vrouwenvelder, C. A. Gorski, B. E. Logan, *Environ. Sci. Technol.* **2020**, *54*, 3628.
[37] S. Cosnier, A. Karyakin, *Electropolymerization: Concepts, Materials and Applications*, John Wiley & Sons, **2011**.
[38] A. J. Heeger, *J. Phys. Chem. B* **2001**, *105*, 8475.
[39] P. J. Kulesza, K. Miecznikowski, M. A. Malik, M. Galkowski, M. Chojak, K. Caban, A. Wieckowski, *Electrochim. Acta* **2001**, *46*, 4065.
[40] A. Lisowska-Oleksiak, A. P. Nowak, *J. Power Sources* **2007**, *173*, 829.
[41] S. Lupu, *Synth. Met.* **2011**, *161*, 384.
[42] Y. Wang, Y. Yang, X. Zhang, C. Liu, X. Hao, *J. Solid State Electrochem.* **2015**, *19*, 3157.
[43] A. A. Ensafi, N. Ahmadi, B. Rezaei, *RSC Adv.* **2015**, *5*, 91448.
[44] J. Niu, W. Yan, J. Du, X. Hao, F. Wang, Z. Wang, G. Guan, *Chem. Eng. J.* **2020**, *389*, 124498.
[45] W. Lövenich, *Polym. Sci., Ser. C* **2014**, *56*, 135.
[46] S. H. Eom, S. Senthilarasu, P. Uthirakumar, S. C. Yoon, J. Lim, C. Lee, H. S. Lim, J. Lee, S.-H. Lee, *Org. Electron.* **2009**, *10*, 536.
[47] F. Bella, L. Porcarelli, D. Mantione, C. Gerbaldi, C. Barolo, M. Grätzel, D. Mecerreyes, *Chem. Sci.* **2020**, *11*, 1485.
[48] L. Fagiolari, E. Varaia, N. Mariotti, M. Bonomo, C. Barolo, F. Bella, *Adv. Sustainable Syst.* **2021**, *5*, 2100025.
[49] T. T. A. Nguyen, B. S. Soram, D. T. Tran, N. H. Kim, J. H. Lee, *Chem. Eng. J.* **2023**, *452*, 139555.
[50] H. Machrafi, F. Iermano, S. Temsamani, I. Bobinac, C. S. Iorio, *Sci. Rep.* **2022**, *12*, 22107.
[51] M. A. A. M. Abdah, M. Mokhtar, L. T. Khoon, K. Sopian, N. A. Dzulkurnain, A. Ahmad, Y. Sulaiman, F. Bella, M. S. Su'ait, *Energy Rep.* **2021**, *7*, 8677.
[52] M. Heydari Gharahcheshmeh, C. T.-C. Wan, Y. Ashraf Gandomi, K. V. Greco, A. Forner-Cuenca, Y.-M. Chiang, F. R. Brushett, K. K. Gleason, *Adv. Mater. Interfaces* **2020**, *7*, 2000855.

[53] K. S. Ryu, Y.-G. Lee, Y.-S. Hong, Y. J. Park, X. Wu, K. M. Kim, M. G. Kang, N.-G. Park, S. H. Chang, *Electrochim. Acta* **2004**, *50*, 843.
[54] M. N. Gueye, A. Carella, J. Faure-Vincent, R. Demadrille, J.-P. Simonato, *Prog. Mater. Sci.* **2020**, *108*, 100616.
[55] K. Sun, S. Zhang, P. Li, Y. Xia, X. Zhang, D. Du, F. H. Isikgor, J. Ouyang, *J. Mater. Sci.: Mater. Electron.* **2015**, *26*, 4438.
[56] L. Niu, C. Kvarnström, A. Ivaska, *J. Electroanal. Chem.* **2004**, *569*, 151.
[57] V.-T. Gruia, A. Ispas, I. Efimov, A. Bund, *J. Solid State Electrochem.* **2020**, *24*, 3231.
[58] G. Li, P. G. Pickup, *Phys. Chem. Chem. Phys.* **2000**, *2*, 1255.
[59] M. J. Donahue, A. Sanchez-Sanchez, S. Inal, J. Qu, R. M. Owens, D. Mecerreyes, G. G. Malliaras, D. C. Martin, *Mater. Sci. Eng., R* **2020**, *140*, 100546.
[60] E. Poverenov, M. Li, A. Bitler, M. Bendikov, *Chem. Mater.* **2010**, *22*, 4019.
[61] A. I. Melato, M. H. Mendonça, L. M. Abrantes, *J. Solid State Electrochem.* **2009**, *13*, 417.
[62] N. Sakmeche, S. Aeiyach, J.-J. Aaron, M. Jouini, J. C. Lacroix, P.-C. Lacaze, *Langmuir* **1999**, *15*, 2566.
[63] A. Forner-Cuenca, E. E. Penn, A. M. Oliveira, F. R. Brushett, *J. Electrochem. Soc.* **2019**, *166*, A2230.
[64] K. V. Greco, A. Forner-Cuenca, A. Mularczyk, J. Eller, F. R. Brushett, *ACS Appl. Mater. Interfaces* **2018**, *10*, 44430.
[65] N. A. Hotaling, K. Bharti, H. Kriel, C. G. Simon, *Biomaterials* **2015**, *61*, 327.
[66] C.-N. Sun, F. M. Delnick, L. Baggetto, G. M. Veith, T. A. Zawodzinski, *J. Power Sources* **2014**, *248*, 560.
[67] S. A. Spanninga, D. C. Martin, Z. Chen, *J. Phys. Chem. C* **2009**, *113*, 5585.
[68] C. Bodart, N. Rossetti, J. Hagler, P. Chevreau, D. Chhin, F. Soavi, S. B. Schougaard, F. Amzica, F. Cicoira, *ACS Appl. Mater. Interfaces* **2019**, *11*, 17226.
[69] F. S. Belaidi, A. Civélas, V. Castagnola, A. Tsopela, L. Mazenq, P. Gros, J. Launay, P. Temple-Boyer, *Sens. Actuators, B* **2015**, *214*, 1.
[70] R. Kiefer, G. A. Bowmaker, R. P. Cooney, P. A. Kilmartin, J. Travas-Sejdic, *Electrochim. Acta* **2008**, *53*, 2593.
[71] X. Peng, L. Peng, C. Wu, Y. Xie, *Chem. Soc. Rev.* **2014**, *43*, 3303.
[72] Y. Shi, L. Peng, Y. Ding, Y. Zhao, G. Yu, *Chem. Soc. Rev.* **2015**, *44*, 6684.
[73] L. Eifert, N. Bevilacqua, K. Köble, K. Fahy, L. Xiao, M. Li, K. Duan, A. Bazylak, P.-C. Sui, R. Zeis, *ChemSusChem* **2020**, *13*, 3154.
[74] J. Zhao, Z. Tu, S. H. Chan, *J. Power Sources* **2021**, *488*, 229434.
[75] I. Zozoulenko, A. Singh, S. K. Singh, V. Gueskine, X. Crispin, M. Berggren, *ACS Appl. Polym. Mater.* **2019**, *1*, 83.
[76] M. Łapkowski, A. Proń, *Synth. Met.* **2000**, *110*, 79.
[77] G. Genchi, A. Carocci, G. Lauria, M. S. Sinicropi, A. Catalano, *Int. J. Environ. Res. Public Health* **2020**, *17*, 679.
[78] J. S. Sudarsan, V. T. Deeptha, D. Maurya, M. Goel, K. R. Kumar, A. Das, *Nat., Environ. Pollut. Technol.* **2015**, *14*, 6.
[79] G. Zotti, S. Zecchin, G. Schiavon, F. Louwet, L. Groenendaal, X. Crispin, W. Osikowicz, W. Salaneck, M. Fahlman, *Macromolecules* **2003**, *36*, 3337.
[80] A. Savva, S. Wustoni, S. Inal, *J. Mater. Chem. C* **2018**, *6*, 12023.
[81] E. R. Nightingale, *J. Phys. Chem.* **1959**, *63*, 1381.
[82] K.-M. Mangold, C. Weidlich, J. Schuster, K. Jüttner, *J. Appl. Electrochem.* **2005**, *35*, 1293.
[83] M. Chen, K. Shafer-Peltier, S. J. Randtke, E. Peltier, *Chem. Eng. J.* **2018**, *344*, 155.